

SUPPLEMENTAL MATERIAL FOR

Ultrathin Two-Dimensional Vertical Ferroelectric Tunneling Junction based on CuInP₂S₆ Monolayer

Min Zhao, Gaoyang Gou,* Xiangdong Ding,* and Jun Sun

Frontier Institute of Science and Technology & State Key Laboratory for Mechanical Behavior of Materials, Xi'an Jiaotong University, Xi'an 710049, People's Republic of China

E-mail: gougaoyang@mail.xjtu.edu.cn; dingxd@mail.xjtu.edu.cn

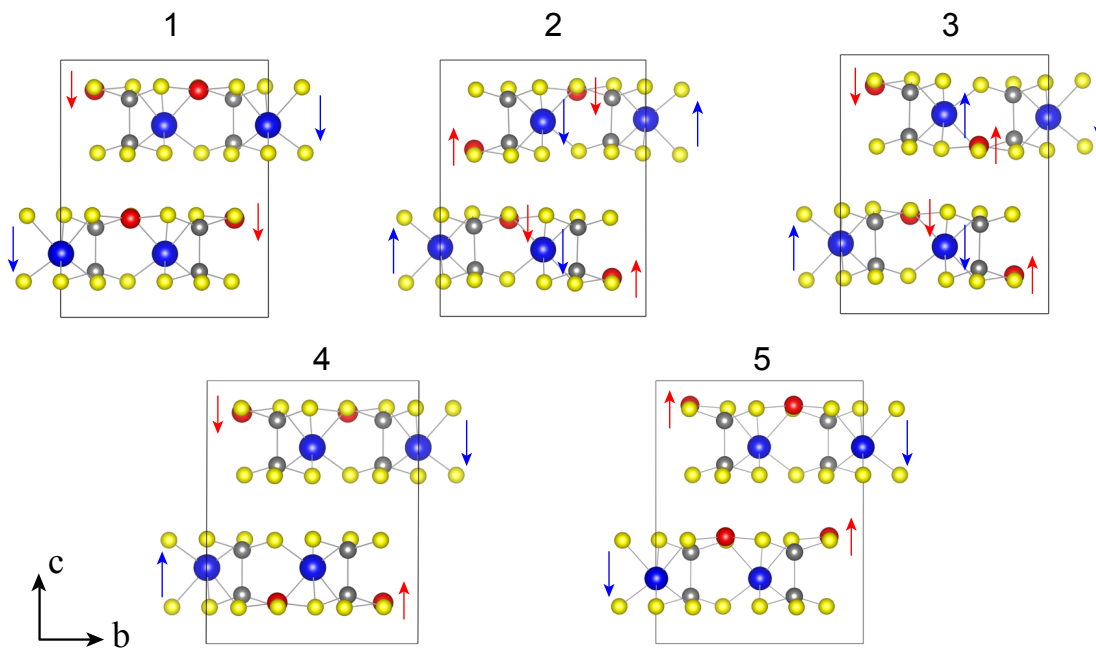


Fig. S1: FE bulk CIPS structural configurations with different Cu occupation patterns and different polar displacement between Cu and In cations. Cu, In, P and S atoms are in red, blue, gray and yellow colors, while polar displacements of Cu and In atoms relative to high symmetric paraelectric reference state are indicated by red and blue arrows respectively.

Table S1: Relative energy for different structural configurations for FE phase of bulk CIPS appeared in Fig.S1.

CuInP ₂ S ₆	1	2	3	4	5
ΔE (meV/cell)	0.00	77.3	9.90	63.3	592.6

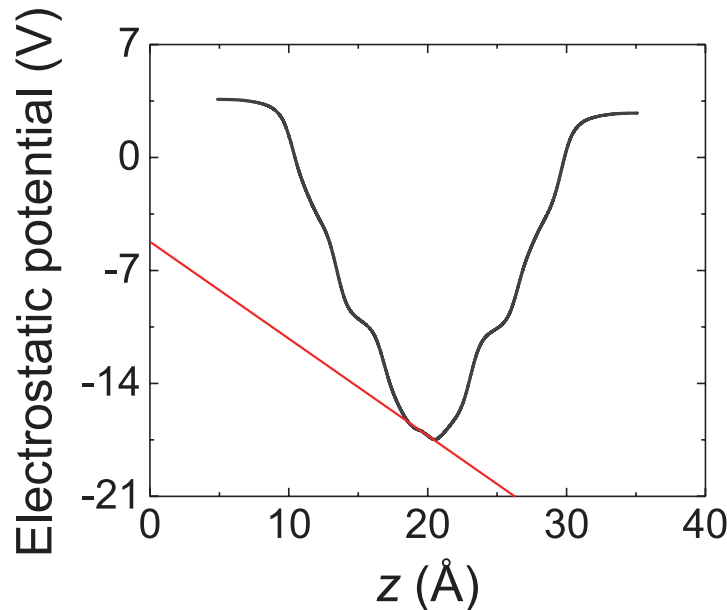


Fig. S2: Depolarization field ϵ_d of CIPS bilayer can be simulated by fitting the slope of macroscopic-averaged electrostatic potential profile along the out-of-plane direction within CIPS bilayer.

Table S2: Our calculated relative energy and net magnetic moment for the nonmagnetic (NM) and hypothetical ferromagnetic (FM) CuInP₂S₆ monolayer.

CuInP ₂ S ₆	NM	FM
ΔE (meV/f.u.)	0.00	-1E-4
μ_{cell} (μ_B)	—	0.00

Table S3: Calculated Born effective charges Z^* for each atom in FE CIPS bulk and monolayer.

Atom	bulk			monolayer			Atom	bulk			monolayer		
	x	y	z	x	y	z		x	y	z	x	y	z
Cu	x	0.29	0.15	-0.07	0.35	0.16	0.00	S	x	-0.81	0.36	-0.42	
	y	-0.17	0.28	0.01	-0.16	0.35	0.00		y	0.10	-2.16	-0.11	
	z	-0.02	0.00	0.61	0.00	0.00	0.40		z	-0.19	0.02	-0.70	
Cu	x	0.29	-0.15	-0.07				S	x	-0.81	-0.36	-0.42	-0.85 -0.37 -0.43
	y	0.17	0.28	-0.01					y	-0.10	-2.16	0.11	-0.10 -2.18 0.11
	z	-0.02	0.00	0.61					z	-0.19	-0.02	-0.70	-0.14 -0.03 -0.72
Cu	x	0.29	0.15	-0.07	0.35	0.16	0.00	S	x	-0.81	0.36	-0.42	
	y	-0.17	0.28	0.01	-0.16	0.35	0.00		y	0.10	-2.16	-0.11	
	z	-0.02	0.00	0.61	0.00	0.00	0.40		z	-0.19	0.02	-0.70	
Cu	x	0.29	-0.15	-0.07				S	x	-0.81	-0.36	-0.42	-0.85 -0.37 -0.43
	y	0.17	0.28	-0.01					y	-0.10	-2.16	0.11	-0.10 -2.18 0.11
	z	-0.02	0.00	0.61					z	-0.19	-0.02	-0.70	-0.14 -0.03 -0.72
In	x	3.99	-0.37	0.02	3.99	-0.39	0.00	S	x	-1.62	0.56	0.32	-1.65 0.56 0.31
	y	0.39	3.99	0.01	0.39	3.99	0.00		y	0.84	-1.34	0.28	0.83 -1.39 0.32
	z	0.05	-0.03	2.09	0.00	0.00	2.18		z	0.08	0.14	-0.65	0.05 0.14 -0.72
In	x	3.99	0.37	0.02				S	x	-1.62	-0.56	0.32	
	y	-0.39	3.99	-0.01					y	-0.84	-1.34	-0.28	
	z	0.05	0.03	2.09					z	0.08	-0.14	-0.65	
In	x	3.99	-0.37	0.02	3.99	-0.39	0.00	S	x	-1.62	0.56	0.32	-1.65 0.56 0.31
	y	0.39	3.99	0.01	0.39	3.99	0.00		y	0.84	-1.34	0.28	0.83 -1.39 0.32
	z	0.05	-0.03	2.09	0.00	0.00	2.18		z	0.08	0.14	-0.65	0.05 0.14 -0.72
In	x	3.99	0.37	0.02				S	x	-1.62	-0.56	0.32	
	y	-0.39	3.99	-0.01					y	-0.84	-1.34	-0.28	
	z	0.05	0.03	2.09					z	0.08	-0.14	-0.65	
P	x	2.77	0.04	0.03	2.79	0.05	0.00	S	x	-2.31	0.38	0.19	-2.29 0.38 0.12
	y	-0.04	2.76	0.03	-0.05	2.79	0.00		y	0.48	-1.27	0.24	0.46 -1.28 0.23
	z	0.00	0.07	0.82	0.00	0.00	0.80		z	0.24	0.19	-0.87	0.18 0.15 -0.72
P	x	2.77	-0.04	0.03				S	x	-2.31	-0.38	0.19	
	y	0.04	2.76	-0.03					y	-0.48	-1.27	-0.24	
	z	0.00	-0.07	0.82					z	0.24	-0.19	-0.87	
P	x	2.77	0.04	0.03	2.79	0.05	0.00	S	x	-2.31	0.38	0.19	-2.29 0.38 0.12
	y	-0.04	2.76	0.03	-0.05	2.79	0.00		y	0.48	-1.27	0.24	0.46 -1.28 0.23
	z	0.00	0.07	0.82	0.00	0.00	0.80		z	0.24	0.19	-0.87	0.18 0.15 -0.72
P	x	2.77	-0.04	0.03				S	x	-2.31	-0.38	0.19	
	y	0.04	2.76	-0.03					y	-0.48	-1.27	-0.24	
	z	0.00	-0.07	0.82					z	0.24	-0.19	-0.87	
P	x	2.78	0.70	-0.01	2.78	0.69	0.00	S	x	-1.14	-0.18	-0.29	
	y	-0.72	2.79	-0.01	-0.69	2.78	0.00		y	-0.28	-2.42	-0.01	
	z	-0.11	-0.05	0.90	0.00	0.00	0.95		z	-0.23	-0.07	-0.78	
P	x	2.78	-0.70	-0.01				S	x	-1.14	0.18	-0.29	-1.17 0.19 -0.26
	y	0.72	2.79	0.01					y	0.28	-2.42	0.01	0.27 -2.40 -0.01
	z	-0.11	0.05	0.90					z	-0.23	0.07	-0.78	-0.23 0.08 -0.72
P	x	2.78	0.70	-0.01	2.78	0.69	0.00	S	x	-1.14	-0.18	-0.29	
	y	-0.72	2.79	-0.01	-0.69	2.78	0.00		y	-0.28	-2.42	-0.01	
	z	-0.11	-0.05	0.90	0.00	0.00	0.95		z	-0.23	-0.07	-0.78	
P	x	2.78	-0.70	-0.01				S	x	-1.14	0.18	-0.29	-1.17 0.19 -0.26
	y	0.72	2.79	0.01					y	0.28	-2.42	0.01	0.27 -2.40 -0.01
	z	-0.11	0.05	0.90					z	-0.23	0.07	-0.78	-0.23 0.08 -0.72
S	x	-2.04	-0.61	0.13	-2.05	-0.59	0.12	S	x	-1.88	0.70	0.12	
	y	-0.34	-0.95	-0.43	-0.33	-0.98	-0.43		y	0.63	-1.68	0.22	
	z	0.12	-0.13	-0.71	0.09	-0.11	-0.72		z	0.07	0.20	-0.71	
S	x	-2.04	0.61	0.13				S	x	-1.88	-0.70	0.12	-1.89 -0.68 0.14
	y	0.34	-0.95	0.43					y	-0.63	-1.68	-0.22	-0.61 -1.68 -0.22
	z	0.12	0.13	-0.71					z	0.07	-0.20	-0.71	0.04 -0.24 -0.72
S	x	-2.04	-0.61	0.13	-2.05	-0.59	0.12	S	x	-1.88	0.70	0.12	-1.89 -0.68 0.14
	y	-0.34	-0.95	-0.43	-0.33	-0.98	-0.43		y	0.63	-1.68	0.22	
	z	0.12	-0.13	-0.71	0.09	-0.11	-0.72		z	0.07	0.20	-0.71	0.04 -0.24 -0.72

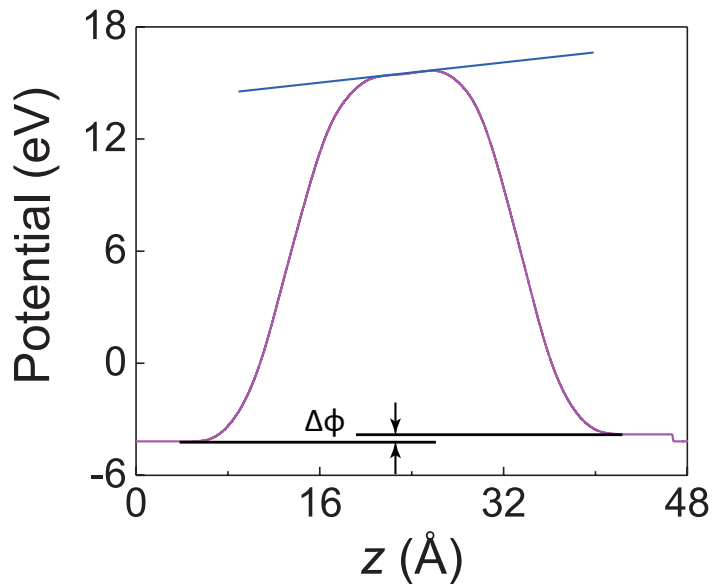


Fig. S3: Macroscopic-averaged electrostatic potential profile for graphene/CIPS bilayer/graphene heterostructure along the out-of-plane direction. Abrupt change of electrostatic potential in vacuum region and the non-zero slope of macroscopic-averaged electrostatic potential within the bilayer region are also indicated.

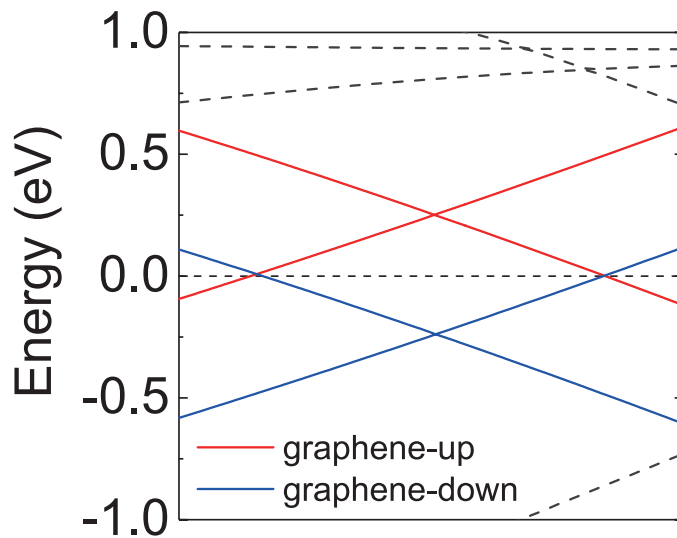


Fig. S4: Band structure for graphene/CIPS monolayer/graphene heterostructure calculated from ATK software. Fermi energy level is set as energy zero.

Table S4: Calculated planar lattice parameter a , b and the overall thickness d for vdW stacking graphene/CIPS monolayer/graphene heterostructure through VASP and ATK softwares respectively.

	VASP	ATK
a (Å)	9.942	9.938
b (Å)	12.791	12.764
d (Å)	10.19	10.07

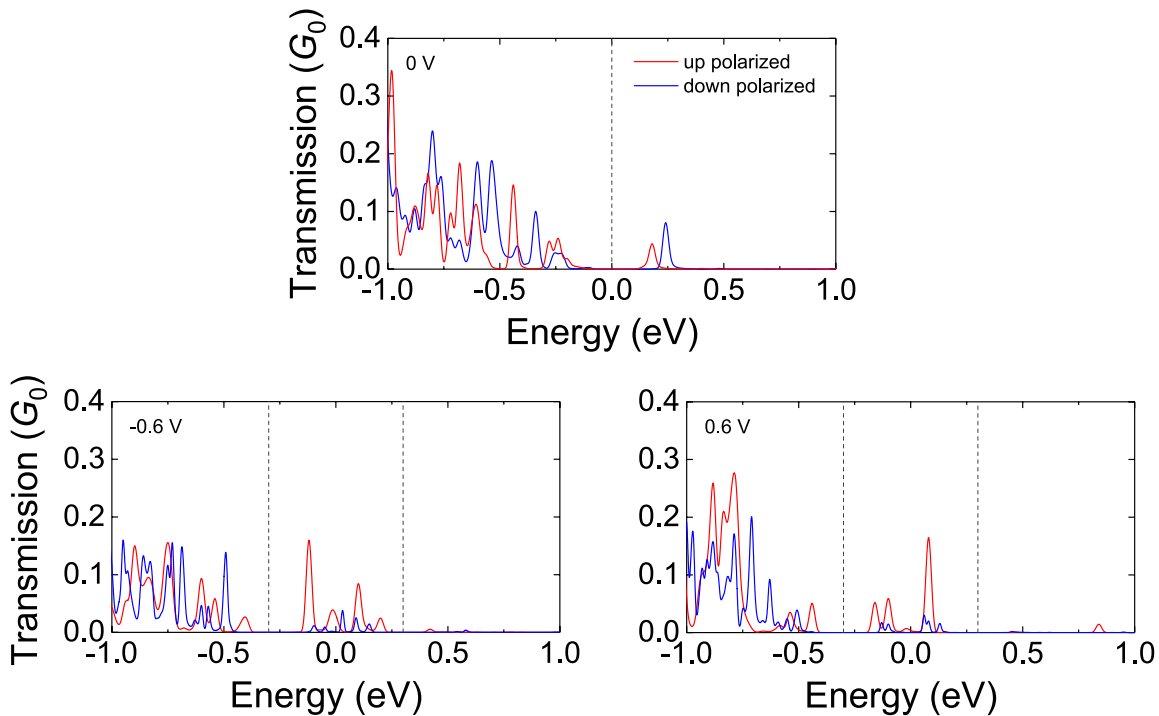


Fig. S5: Our simulated tunneling transmission spectrum for graphene/CIPS monolayer/graphene FTJ device under different bias voltage, where FTJ device with upwards and downwards oriented FE polarization are included for simulations. The vertical dashed line represents energy range corresponding to the bias voltage window.

Table S3 summarizes our calculated Born effective charge Z^* for all atoms along different Cartesian axes in FE CIPS bulk and monolayer. Similar to FE polarization, Born effective charges are also nearly independent on system dimension, as corresponding Z^* only changes slightly from the bulk to monolayer. In and S ions have planar Z^* in larger magnitudes (i. e. 3.99 and -2.42) than their nominal valence states, indicating the strong covalent character for In-S bond. It is noted that all cations in CIPS have the out-of-plane Z^* values smaller than their nominal valence states, which is likely due the negative piezoelectricity effect of FE CIPS system.¹ Typically, we predict out-of-plane $Z^* = 1.63$ for Bi cation in BiTeCl monolayer, a prototypical 2D material with negative piezoelectric response,² which is also smaller than its nominal valence state.

Fig.S3 and Table S4 summarize the energy band structure and lattice parameters for graphene/CIPS monolayer/graphene heterostructure calculated using ATK software. Obviously, ATK can predict similar electronic and structural results, as compared to VASP.

Transport properties such as $I - V$ curve is further simulated using a self-consistent approach with the combination of DFT and non-equilibrium Green's function (NEGF) formalism as implemented in the ATK package.³⁻⁵ Electron transmission through the scattering region is described by the Landauer–Büttiker formula⁶ and the transmission current can be obtained self-consistently under a given bias voltage. The double- ζ -polarized(DZP) basis set is adopted for electron wave function expansion. The Brillouin zone of graphene/CIPS monolayer/graphene FTJ device is sampled using a $5 \times 2 \times 51$ Monkhorst-Pack \mathbf{k} -point mesh. The PBEsol functional is also employed for transport properties calculations and the electron temperature is set to be 300K.

References

- (1) You, L.; Zhang, Y.; Zhou, S.; Chaturvedi, A.; Morris, S. A.; Liu, F.; Chang, L.; Ichinose, D.; Funakubo, H.; Hu, W.; Wu, T.; Liu, Z.; Dong, S.; Wang, J. Origin of giant negative

- piezoelectricity in a layered van der Waals ferroelectric. *Sci. Adv.* **2019**, *5*, 3780.
- (2) Kim, J.; Rabe, K. M.; Vanderbilt, D. Negative piezoelectric response of van der Waals layered bismuth tellurohalides. *Phys. Rev. B* **2019**, *100*, 104115.
- (3) QuantumATK 2016.4, Synopsys QuantumATK. <https://www.synopsys.com/silicon/quantumatk.html>.
- (4) Brandbyge, M.; Mozos, J.; Ordejón, P.; Taylor, J.; Stokbro, K. Density-functional method for nonequilibrium electron transport. *Phys. Rev. B* **2002**, *65*, 165401.
- (5) Taylor, J.; Guo, H.; Wang, J. Ab initio modeling of quantum transport properties of molecular electronic devices. *Phys. Rev. B* **2001**, *63*, 245407.
- (6) Landauer, R. Spatial Variation of Currents and Fields Due to Localized Scatterers in Metallic Conduction. *IBM J. Res. Dev.* **1957**, *1*, 223–231.